4

Mantle Temperatures and Thermodynamic Properties

4.1 Heat Conduction and the Age of the Earth

4.1.1 Cooling of an Isothermal Earth

Determinations of the temperature distribution within the Earth have long been a major focus of the physical sciences. Early in the nineteenth century it was recognized from temperature measurements in mines, that the temperature T increased with depth y at a rate $dT/dy = 20$–$30 \, \mathrm{K \, km^{-1}}$, the geothermal gradient. At that time, the heat flow at the Earth's surface implied by the geothermal gradient was attributed to the secular cooling of the planet, an inference that, as it turns out, was partially correct.

William Thompson (later Lord Kelvin) (Figure 4.1) used this assumption as the basis for his estimate of the age of the Earth (Burchfield, 1975). Thompson assumed that the Earth was conductively cooling from a hot initial state. He applied solutions for the cooling of a

Figure 4.1. Photograph of William Thompson (Lord Kelvin).

semi-infinite half-space to determine the time required to establish the present geothermal gradient. The distribution of temperature T at shallow depths can be modeled as one-dimensional, time-dependent heat conduction in the absence of heat sources (see Chapter 6):

$$\rho c \frac{\partial T}{\partial t} = k \frac{\partial^2 T}{\partial y^2} \tag{4.1.1}$$

In this heat conduction equation, ρ is the density, c is the specific heat, k is the thermal conductivity, y is the depth, and t is time. We consider a semi-infinite half-space defined by $y > 0$ which is initially at a temperature T_1. At $t = 0$, the surface $y = 0$ is instantaneously subjected to the temperature T_0 and the surface temperature is held at T_0 for $t > 0$.

The solution to this problem, which serves as the basic thermal model of the oceanic lithosphere, is best obtained by introducing the nondimensional similarity variables

$$\theta = \frac{T_1 - T}{T_1 - T_0} \tag{4.1.2}$$

$$\eta = \frac{y}{2 (\kappa t)^{1/2}} \tag{4.1.3}$$

where $\kappa = k/\rho c$ is the thermal diffusivity. The solutions at different times are "similar" to each other in the sense that the spatial dependence at one time can be obtained from the spatial dependence at a different time by stretching the coordinate y by the square root of the ratio of the times.

Derivatives with respect to the variables t and y transform to derivatives with respect to the variable η using the chain rule as follows:

$$\frac{\partial \theta}{\partial t} = \frac{d\theta}{d\eta} \frac{\partial \eta}{\partial t} = \frac{d\theta}{d\eta} \left(-\frac{1}{4} \frac{y}{\sqrt{\kappa t}} \frac{1}{t} \right) = \frac{d\theta}{d\eta} \left(-\frac{1}{2} \frac{\eta}{t} \right) \tag{4.1.4}$$

$$\frac{\partial \theta}{\partial y} = \frac{d\theta}{d\eta} \frac{\partial \eta}{\partial y} = \frac{d\theta}{d\eta} \frac{1}{2\sqrt{\kappa t}} \tag{4.1.5}$$

$$\frac{\partial^2 \theta}{\partial y^2} = \frac{1}{2\sqrt{\kappa t}} \frac{d^2\theta}{d\eta^2} \frac{\partial \eta}{\partial y} = \frac{1}{4} \frac{1}{\kappa t} \frac{d^2\theta}{d\eta^2} \tag{4.1.6}$$

Substitution of (4.1.2) to (4.1.6) into (4.1.1) gives

$$-\eta \frac{d\theta}{d\eta} = \frac{1}{2} \frac{d^2\theta}{d\eta^2} \tag{4.1.7}$$

with the boundary conditions

$$\theta = 1 \ \text{ at } \ \eta = 0 \tag{4.1.8}$$

$$\theta = 0 \ \text{ as } \ \eta \to \infty \tag{4.1.9}$$

The introduction of the similarity variable reduces the partial differential equation (4.1.1) to an ordinary differential equation (4.1.7) in the variable η. This is appropriate as long as the similarity solution satisfies the required boundary conditions expressed as (4.1.8) and (4.1.9) in terms of the similarity variables.

Equation (4.1.7) can be integrated by letting

$$\phi = \frac{d\theta}{d\eta} \tag{4.1.10}$$

Upon rewriting (4.1.7) we obtain

$$-\eta \, d\eta = \frac{1}{2} \frac{d\phi}{\phi} \tag{4.1.11}$$

Integration is straightforward with the result

$$-\eta^2 = \ln \phi - \ln c_1 \tag{4.1.12}$$

where $-\ln c_1$ is the constant of integration. It follows that

$$\phi = c_1 e^{-\eta^2} = \frac{d\theta}{d\eta} \tag{4.1.13}$$

Upon integration we obtain

$$\theta = c_1 \int_0^\eta e^{-\eta'^2} \, d\eta' + 1 \tag{4.1.14}$$

where η' is a dummy variable of integration and the condition $\theta(0) = 1$ was used to evaluate the second constant of integration. Since $\theta(\infty) = 0$, we must have

$$0 = c_1 \int_0^\infty e^{-\eta'^2} \, d\eta' + 1 \tag{4.1.15}$$

The definite integral is

$$\int_0^\infty e^{-\eta'^2} \, d\eta' = \frac{\sqrt{\pi}}{2} \tag{4.1.16}$$

Thus the constant $c_1 = -2/\sqrt{\pi}$ and

$$\theta = 1 - \frac{2}{\sqrt{\pi}} \int_0^\eta e^{-\eta'^2} \, d\eta' \tag{4.1.17}$$

The definite integral is the definition of the error function

$$\operatorname{erf}(\eta) \equiv \frac{2}{\sqrt{\pi}} \int_0^\eta e^{-\eta'^2} \, d\eta' \tag{4.1.18}$$

Thus we can rewrite θ as

$$\theta = 1 - \operatorname{erf}(\eta) = \operatorname{erfc}(\eta) \tag{4.1.19}$$

where $\operatorname{erfc}(\eta)$ is the complementary error function. Values of the error function and the complementary error function are listed in Table 4.1; the functions are also shown in Figure 4.2.

The solution for the temperature as a function of time t and depth y is (4.1.19). It can be written in terms of the original variables as

$$\frac{T_1 - T}{T_1 - T_0} = \operatorname{erfc}\left(\frac{y}{2\sqrt{\kappa t}}\right) \tag{4.1.20}$$

Table 4.1. *The Error Function and the
Complementary Error Function*

η	erf η	erfc η
0	0	1.0
0.02	0.022565	0.977435
0.04	0.045111	0.954889
0.06	0.067622	0.932378
0.08	0.090078	0.909922
0.10	0.112463	0.887537
0.15	0.167996	0.832004
0.20	0.222703	0.777297
0.25	0.276326	0.723674
0.30	0.328627	0.671373
0.35	0.379382	0.620618
0.40	0.428392	0.571608
0.45	0.475482	0.524518
0.50	0.520500	0.479500
0.55	0.563323	0.436677
0.60	0.603856	0.396144
0.65	0.642029	0.357971
0.70	0.677801	0.322199
0.75	0.711156	0.288844
0.80	0.742101	0.257899
0.85	0.770668	0.229332
0.90	0.796908	0.203092
0.95	0.820891	0.179109
1.0	0.842701	0.157299
1.1	0.880205	0.119795
1.2	0.910314	0.089686
1.3	0.934008	0.065992
1.4	0.952285	0.047715
1.5	0.966105	0.033895
1.6	0.976348	0.023652
1.7	0.983790	0.016210
1.8	0.989091	0.010909
1.9	0.992790	0.007210
2.0	0.995322	0.004678
2.2	0.998137	0.001863
2.4	0.999311	0.000689
2.6	0.999764	0.000236
2.8	0.999925	0.000075
3.0	0.999978	0.000022

At $y = 0$, the complementary error function is 1 and $T = T_0$. As $y \rightarrow \infty$ or $t = 0$, erfc is 0 and $T = T_1$. The general solution for θ or $(T_1 - T)/(T_1 - T_0)$ is shown as erfc (η) in Figure 4.2.

Regions in the Earth in which heat diffusion is an important heat transfer mechanism are usually referred to as thermal boundary layers. In this case the thickness of the thermal boundary layer requires an arbitrary definition, since the temperature T approaches the initial
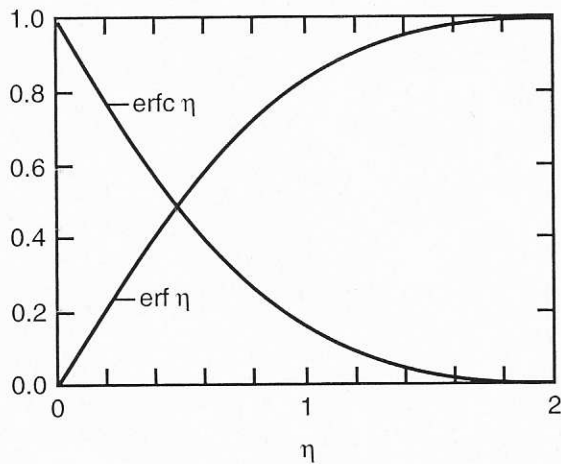
Figure 4.2. The error function erf η and the complementary error function erfc η as a function of η.

temperature T_1 asymptotically. We define the thickness of the boundary layer y_T as the value of y where $\theta = 0.1$. This thickness increases with time as the half-space cools. However, the condition $\theta = 0.1$ defines a unique value of the similarity variable η_T. From (4.1.19) and Table 4.1 we obtain

$$\eta_T = \mathrm{erfc}^{-1}(0.1) = 1.16 \tag{4.1.21}$$

and from (4.1.3) we get

$$y_T = 2\eta_T\sqrt{\kappa t} = 2.32\sqrt{\kappa t} \tag{4.1.22}$$

The thickness of the thermal boundary layer is 2.32 times the characteristic thermal diffusion distance $\sqrt{\kappa t}$.

The heat flux q_0 at the surface $y = 0$ is given by differentiating (4.1.20) according to Fourier's law of heat conduction and evaluating the result at $y = 0$:

$$q_0 = k\left(\frac{\partial T}{\partial y}\right)_{y=0} = \frac{k\,(T_1 - T_0)}{2\sqrt{\kappa t}}\,\frac{d}{d\eta}\,(\mathrm{erf}\,\eta)_{\eta=0}$$

$$= \frac{k\,(T_1 - T_0)}{\sqrt{\pi\kappa t}} \tag{4.1.23}$$

Equation (4.1.23) shows that the surface heat flux is proportional to the product of conductivity k and the temperature difference $(T_1 - T_0)$ and inversely proportional to the thermal boundary layer thickness. With the standard definition $q = -k\,(\partial T/\partial y)$, the upward heat loss would be negative. Since the Earth's surface heat flow is always taken to be a positive quantity, the minus sign is not included in (4.1.23).

On the basis of (4.1.23), Thompson proposed that the age of the Earth t_0 is given by

$$t_0 = \frac{(T_1 - T_0)^2}{\pi\kappa\,(\partial T/\partial y)_0^2} \tag{4.1.24}$$

where $(\partial T/\partial y)_0$ is the present geothermal gradient. With $(\partial T/\partial y)_0 = 25\,\mathrm{K\,km^{-1}}$, $T_1 - T_0 = 2{,}000\,\mathrm{K}$, and $\kappa = 1\,\mathrm{mm^2\,s^{-1}}$, the age of the Earth from (4.1.24) is $t_0 = 65\,\mathrm{Myr}$. Thompson arrived at this age using the geothermal gradient measured in mines. The values of the temperature difference and the thermal diffusivity used were also reasonable. Based on the

laws of physics known at that time, the mid-nineteenth century, the age given by Thompson was reasonable. We now recognize, however, that the continental crust has a near-steady-state heat balance due to the heat generated by the heat-producing isotopes within the crust and the mantle heat flux from below. Ironically, had Thompson known to apply the model to the oceanic lithosphere, he would have obtained very nearly its correct mean age.

4.1.2 Cooling of a Molten Earth

Thompson later modified the conductive cooling model of the Earth to include the hypothesis that its interior was initially molten. The existence of many surface volcanoes suggested to him that the Earth was cooling from an initially molten state. In order to model the solidification problem he considered the instantaneous cooling of a semi-infinite fluid half-space initially at the solidification temperature. The solution to this problem had been given by Stefan (1891).

The solidification problem is illustrated in Figure 4.3. The melt has solidified to the depth $y = y_m(t)$. We assume that there is molten material of uniform temperature T_m everywhere below the growing solid surface layer. The fact that the molten region does not extend infinitely far below the surface is of no consequence for the solution. We solve the heat conduction equation (4.1.1) in the interval $0 \le y \le y_m(t)$ subject to the conditions $T = T_0$ at $y = 0$, $T = T_m$ at $y = y_m(t)$, and $y_m = 0$ at $t = 0$. The position of the solidification boundary is a priori an unknown function of time. As in the case of the sudden cooling of a semi-infinite half-space, there is no length scale in this problem. For this reason, we once again introduce the dimensionless coordinate $\eta = y/2\sqrt{\kappa t}$ as in (4.1.3); it is also convenient to introduce the dimensionless temperature $\theta = (T - T_0)/(T_m - T_0)$ similar to (4.1.2).

The dimensionless coordinate η is obtained by scaling the depth with the thermal diffusion length $\sqrt{\kappa t}$ since there is no other length scale in the problem. Similarly, the depth of the solidification interface y_m must also scale with the thermal diffusion length in such a way that $y_m/\sqrt{\kappa t}$ is a constant. In other words, the depth of the solidification boundary increases with time proportionately with the square root of time. We have used dimensional arguments to determine the functional form of the dependence of y_m on t, a nontrivial result. Since $\eta = y/2\sqrt{\kappa t}$ and y_m is proportional to $\sqrt{\kappa t}$, the solidification boundary corresponds to a constant value $\eta_m = y_m/2\sqrt{\kappa t}$ of the similarity coordinate η. We denote this constant value by $\eta_m = \lambda$. Thus we have

$$y_m = 2\lambda\sqrt{\kappa t} \tag{4.1.25}$$

Figure 4.3. Growth of a solid layer at the surface of a solidifying magma. The surface $y = 0$ is maintained at $T = T_0$. Initially the half-space $y > 0$ contains a magma at its melt temperature T_m. The lower boundary of the solid layer $y = y_m(t)$ is shown.
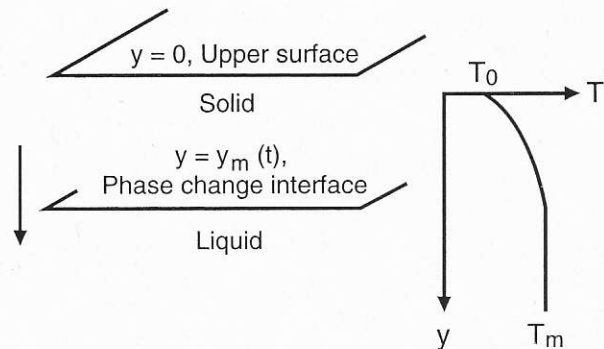
With our definitions of θ and η it is clear that the heat conduction equation for $\theta(\eta)$ is identical with (4.1.7), whose solution we already know to be proportional to $\mathrm{erf}(\eta)$. This form of solution automatically satisfies the condition $\theta = 0(T = T_0)$ on $\eta = 0(y = 0)$. To satisfy the remaining condition that $\theta = 1(T = T_m)$ at $\eta = \eta_m(y = y_m) = \lambda$, we need simply choose the constant of proportionality appropriately. The solution is

$$\theta = \frac{\mathrm{erf}(\eta)}{\mathrm{erf}(\lambda)} \tag{4.1.26}$$

which gives the temperature in the solidified layer $0 \leq y \leq y_m$. In the molten region $y > y_m$, $T = T_m$.

The constant λ is determined by requiring that the latent heat liberated at the solidification boundary be conducted vertically upward, away from the interface. In time δt, the interface moves downward a distance $(dy_m/dt)\delta t$. In so doing, a mass per unit area $\rho(dy_m/dt)\delta t$ is solidified, thus releasing an amount of latent heat $\rho L(dy_m/dt)\delta t$ per unit area (L is the latent heat liberated upon solidification per unit mass). Conservation of energy requires that this heat release be conducted away from the boundary at precisely the rate at which it is liberated. The heat cannot be conducted downward because the magma is at a constant temperature. Fourier's law of heat conduction gives the rate of upward heat conduction per unit time and per unit area at $y = y_m$ as $k(\partial T/\partial y)_{y=y_m}$. Multiplication of this by δt and equating it to $\rho L(dy_m/dt)\delta t$ gives the equation for finding λ:

$$\rho L \frac{dy_m}{dt} = k\left(\frac{\partial T}{\partial y}\right)_{y=y_m} \tag{4.1.27}$$

From (4.1.25) the speed of the solidification boundary is

$$\frac{dy_m}{dt} = \frac{\lambda\sqrt{\kappa}}{\sqrt{t}} \tag{4.1.28}$$

and the temperature gradient at $y = y_m$ is

$$\left(\frac{\partial T}{\partial y}\right)_{y=y_m} = \left(\frac{d\theta}{d\eta}\right)_{\eta=\eta_m=\lambda}\left(\frac{\partial \eta}{\partial y}\right)(T_m - T_0)$$

$$= \frac{(T_m - T_0)}{2\sqrt{\kappa t}}\frac{2}{\sqrt{\pi}}e^{-\lambda^2}\frac{1}{\mathrm{erf}(\lambda)} \tag{4.1.29}$$

Substitution of (4.1.28) and (4.1.29) into (4.1.27) gives

$$\frac{L\sqrt{\pi}}{c(T_m - T_0)} = \frac{e^{-\lambda^2}}{\lambda\,\mathrm{erf}(\lambda)} \tag{4.1.30}$$

a transcendental equation for determining λ. Given a numerical value of the left side of (4.1.30), λ can be found by iteratively calculating the right side of the equation until agreement is found. Alternatively, the right side of (4.1.30) can be plotted as a function of λ, as in Figure 4.4, and the solution for a particular value of the left side of the equation can be found graphically.

On the basis of the solution to the solidification problem, the age of the Earth is given by

$$t_0 = \frac{(T_m - T_0)^2}{\pi\kappa\,(\partial T/\partial y)_0^2\,\mathrm{erf}^2(\lambda)} \tag{4.1.31}$$

Figure 4.4. The right side of the transcendental equation (4.1.30) for determining the growth of a solid layer at the surface of a solidifying magma as a function of λ.
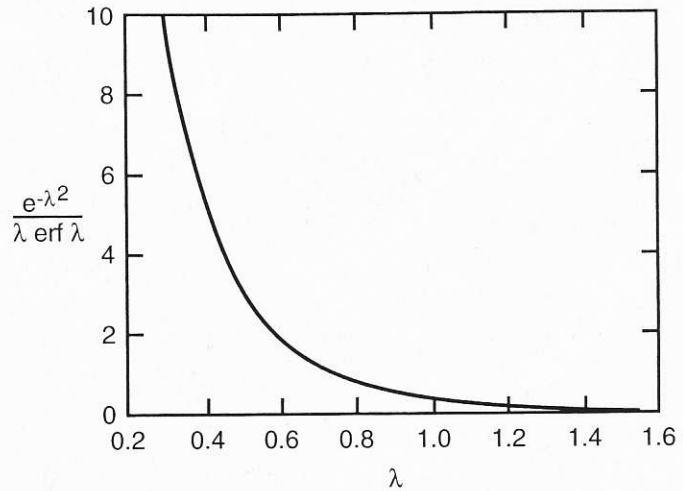
By comparing (4.1.31) and (4.1.24) we see that solidification increases the estimate of the age of the Earth by the factor $1/\mathrm{erf}^2(\lambda)$. For $L = 400\,\mathrm{kJ\,kg}^{-1}$, $c = 1\,\mathrm{kJ\,kg}^{-1}\,\mathrm{K}^{-1}$, and $T_m - T_0 = 2{,}000\,\mathrm{K}$, we find from (4.1.30) that $\lambda = 1.06$ and $\mathrm{erf}(\lambda) = 0.865$. Thus, including solidification increases the estimate of the age of the Earth by a factor of 4/3.

The calculations made by William Thompson were front page news in the London papers of the time and a debate raged over the age of the Earth. On one side were the clergy of the Church of England led by Bishop Wilburforce, who interpreted the Bible as giving an age of the Earth of some 4,000 yr. On the other side were the noted geologists of the day led by James Hutton, who argued that the sedimentary and fossil records required a much greater age for the Earth. However, they could not place quantitative limits on their estimates and much of the scientific establishment of the day accepted Thompson's estimate of the Earth's age, 50–100 Myr, as more reliable since it was based on seemingly reasonable theoretical arguments.

It was only with the discovery of radioactive elements and the implications for heat sources distributed within the Earth that a new approach to the thermal structure of the Earth was taken. Holmes (1915a,b, 1916) not only suggested that the decay of radioactive elements heated the interior of the Earth, but he also used their decay constants to suggest that the age of the Earth was billions of years.

4.1.3   *Conductive Cooling with Heat Generation*

The concept of secular cooling was subsequently replaced by the concept of a steady-state heat balance. The heat flux from the interior of the Earth was thought to be balanced with the heat generated by the decay of the radioactive elements. The most popular model involved a near-surface layer of thickness y_1 with a uniform rate of heat production per unit mass H overlying an interior totally depleted in the heat-producing elements. Again it was assumed that heat transport was by conduction.

On the assumption that heat is transported (conducted) only in the vertical direction and that there are no time variations, the heat conduction equation with heat sources can be written as

$$0 = k \frac{d^2 T}{dy^2} + \rho H \tag{4.1.32}$$

For the boundary conditions $T = T_0$ at $y = 0$ and $dT/dy = 0$ at $y = y_1$, (4.1.32) can be integrated to give

$$T = T_0 + \frac{\rho H}{k}\left(y_1 y - \frac{y^2}{2}\right) \tag{4.1.33}$$

If, in addition, the temperature at the base of the layer is prescribed to be the mantle temperature T_1, we have

$$Hy_1^2 = \frac{2k(T_1 - T_0)}{\rho} \tag{4.1.34}$$

Since the surface thermal gradient $(dT/dy)_0$ can also be prescribed, we find

$$y_1 = \frac{2(T_1 - T_0)}{(dT/dy)_0} \tag{4.1.35}$$

$$H = \frac{k}{2\rho(T_1 - T_0)}\left(\frac{dT}{dy}\right)_0^2 \tag{4.1.36}$$

$$T = T_0 + y\left(\frac{dT}{dy}\right)_0\left[1 - \frac{y}{4(T_1 - T_0)}\left(\frac{dT}{dy}\right)_0\right] \tag{4.1.37}$$

For $T_1 - T_0 = 1{,}300\,\text{K}$ and $(dT/dy)_0 = 25\,\text{K}\,\text{km}^{-1}$, (4.1.35) gives $y_1 = 104\,\text{km}$. Further, for $\rho = 3{,}300\,\text{kg}\,\text{m}^{-3}$ and $k = 3.3\,\text{W}\,\text{m}^{-1}\,\text{K}^{-1}$, (4.1.36) gives $H = 2.40 \times 10^{-10}\,\text{W}\,\text{kg}^{-1}$. The resulting temperature profile is given in Figure 4.5. The thickness of the layer is about a factor of 3 larger than the thickness of the continental crust, but the concentration of heat-producing elements is very nearly that of typical continental rocks.

The basic hypothesis of an upward concentration of heat-producing elements with steady-state heat conduction was the generally accepted explanation for the temperature distribution in the Earth's interior from about 1920 to the late 1960s. It provided an explanation for the
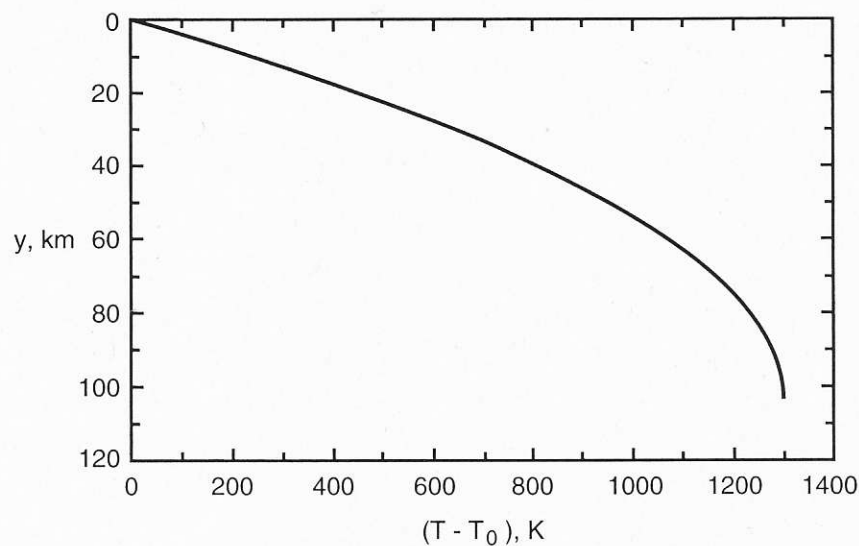
Figure 4.5. Near-surface temperature distribution in the Earth assuming a conduction profile with the heat-producing elements uniformly distributed in the region $0 < y < y_1$. On the assumption that $dT/dy = 0$ at $y = y_1$ and for $(dT/dy)_0 = 25\,\text{K}\,\text{km}^{-1}$, $T_1 - T_0 = 1{,}300\,\text{K}$, we have $y_1 = 104\,\text{km}$ and $H = 2.4 \times 10^{-10}\,\text{W}\,\text{kg}^{-1}$.

temperature gradient in the continental crust, but allowed for the solid upper mantle required by seismic studies.

The hypothesis that the heat-producing elements were strongly concentrated in the crust led to the prediction that the surface heat flow in the oceans, where the crust was known to be thin, would be considerably lower than the surface heat flow in the continents. Measurements by Revelle and Maxwell (1952) in the Pacific and by Bullard (1954) in the Atlantic showed that oceanic heat flow was very nearly equal to continental heat flow, so the prediction was not valid. Bullard et al. (1956) attributed this equality of heat flow to mantle convection. Nevertheless it took another 15 years before the model with an upward concentration of heat sources and steady-state heat conduction was discarded.

4.1.4 Mantle Convection and Mantle Temperatures

The acceptance of mantle convection in the late 1960s provided a natural explanation for the high thermal gradients near the Earth's surface; they are a consequence of thermal boundary layers associated with mantle convection. Beneath the boundary layers heat transport is primarily by convection and the thermal gradient at depth is nearly adiabatic.

Three distinct thermal regimes thus occur within the mantle–crust system (Jeanloz and Morris, 1986). First, there are nearly adiabatic regions, where advective heat transport by vertical motion dominates all other heat transfer mechanisms. Most of the lower mantle appears to be in this category, as are the upper mantle beneath the lithosphere and portions of the transition zone – roughly 90% of the mantle (Ito and Katsura, 1989). Practically all of the outer core is in this category as well. These regions are characterized by nearly isentropic (adiabatic) radial variations of temperature. Second, there are regions where heat transfer by advection is roughly equal to heat transport by conduction. These are the thermal boundary layers described in the previous section. Included in this category are oceanic lithosphere, part of the D'' layer at the base of the mantle, and part of the subcrustal lithosphere beneath continents. There also may be interfacial thermal boundary layers within the transition zone. Finally, there are regions where conductive heat transport dominates, called conduction layers. The continental crust and the upper mantle attached to it are the most important examples of this group. Altogether, conductive layers comprise less than 2% of the volume of the Earth.

Mantle convection can account for virtually all of the known temperature structure in the nearly adiabatic advective regions and thermal boundary layers. Taking into consideration the near-surface concentration of radioactive heat sources, it is possible to explain temperatures in the continental crust as well. This is certainly one of the major successes of convection theory.

The precision with which temperatures are known degrades with depth, and reflects the increased uncertainty in composition and thermodynamic parameters in the deep mantle and core. At the present time, lithospheric temperatures can be estimated to within about $\pm 10\%$. The uncertainty increases with depth, and in the lower mantle and the core reaches perhaps $\pm 30\%$, or about $\pm 1,000\,\text{K}$. Unlike seismic structure, lateral variations in temperature are not small perturbations to the spherically averaged geotherm. In the upper mantle, lateral temperature variations approach $\pm 50\%$ of the spherical average temperature. The three-dimensional thermal structure of the mantle is closely connected to the pattern of mantle convection. Anomalously high temperatures are associated with regions of ascending flow, while anomalously low temperatures characterize regions with descending flow, such as subduction zones.

In addition to temperature, an understanding of mantle convection requires a knowledge of other thermodynamic parameters and properties, including density ρ, pressure p, specific heats c_p and c_v, thermal expansivity α, thermal conductivity k, thermal diffusivity κ, and the Grüneisen parameter γ. The thermodynamic properties of mantle phase transformations, including solid–solid and solid–liquid reactions, are also important. Some of these parameters are reasonably well constrained for the upper mantle by laboratory measurements and inferences drawn from geophysical data. At greater depths, however, the situation changes. Some properties, such as density, are known from seismology, while others, such as the specific heats, are well constrained by solid-state theory. Others, such as thermal conductivity, are poorly known.

4.1.5 Surface Heat Flow and Internal Heat Sources

Heat escaping from the Earth's interior is, in large part, brought to the surface by mantle convection. The Earth's surface heat loss is therefore a directly observable measure of its internal convective activity and thermal structure. The total heat flow from the interior of the Earth Q is given by

$$Q = \overline{q}_c A_c + \overline{q}_o A_o \qquad (4.1.38)$$

where $\overline{q}_c$ is the mean continental heat flux, A_c is the area of the continents, $\overline{q}_o$ is the mean oceanic heat flux, and A_o is the area of the oceans. The distribution of the Earth's surface heat flux has been shown in Figure 2.8; values of $\overline{q}_c$ and $\overline{q}_o$ have been given by Pollack et al. (1993). The area of the continents, including the continental margins, is $A_c = 2 \times 10^8 \text{ km}^2$. Multiplication of this by $\overline{q}_c = 65 \text{ mW m}^{-2}$ gives the total heat flow from the continents $Q_c = 1.30 \times 10^{13} \text{ W}$. The area of the oceans, including the marginal basins, is $A_o = 3.1 \times 10^8 \text{ km}^2$. Multiplication of this by $\overline{q}_o = 101 \text{ mW m}^{-2}$ gives the total heat flow from the oceans $Q_o = 3.13 \times 10^{13} \text{ W}$. With $Q = Q_o + Q_c$, we find Q equal to $4.43 \times 10^{13} \text{ W}$. Accordingly, the mean surface heat flow for the Earth $\overline{q}_s$ is given by $4.43 \times 10^{13} \text{ W}$ divided by the Earth's surface area of $5.1 \times 10^8 \text{ km}^2$, or $\overline{q}_s = 87 \text{ mW m}^{-2}$.

A substantial part of the heat lost through the Earth's surface originates in the interior of the Earth by the decay of the radioactive elements uranium, thorium, and potassium. Some part of the surface heat loss must also come from the overall cooling of the Earth through geologic time. An upper limit to the concentration of radioactive elements in the Earth can be derived by attributing all the surface heat loss to the radioactive heat generation. The upper bound to the mean heat generation per unit mass H is then given by

$$H = \frac{Q}{M} \qquad (4.1.39)$$

where M is the mass of the heat-producing material in the Earth. If we assume that the entire mass of the Earth, $5.97 \times 10^{24} \text{ kg}$, is involved in radiogenic heat generation and take $Q = 4.43 \times 10^{13} \text{ W}$, we find an upper bound of $H = 7.42 \times 10^{-12} \text{ W kg}^{-1}$. However, on the basis of geochemical studies, it can be argued that the core cannot contain a significant fraction of the heat-producing elements in the Earth. In this case, the mass in (4.1.39) should be the mass of the mantle, $4.0 \times 10^{24} \text{ kg}$, and the upper bound becomes $H = 11.1 \times 10^{-12} \text{ W kg}^{-1}$.

A reduction must be made in the value of H appropriate to the mantle, since a substantial fraction of the heat lost from the continents originates in the highly concentrated radioactive isotopes of the continental crust. We estimate that of the mean continental heat flux of $65\,\text{mW}\,\text{m}^{-2}$, $28\,\text{mW}\,\text{m}^{-2}$ can be attributed to the mantle and $37\,\text{mW}\,\text{m}^{-2}$ to radioactive isotopes in the crust. This crustal contribution corresponds to a total heat flow of $7.4 \times 10^{12}\,\text{W}$, or 17% of the total surface heat flow. Reduction of the mantle heat production by this amount gives $H = 9.22 \times 10^{-12}\,\text{W}\,\text{kg}^{-1}$ as an upper bound to the mean heat generation rate per unit mass of the mantle.

Only a fraction of the Earth's present surface heat flow can be attributed to the decay of radioactive isotopes presently in the mantle. Since the radioactive isotopes decay into stable isotopes, heat production due to radioactive decay decreases with time. For example, we show below that the heat production three billion years ago was about twice as great as it is today. Because less heat is being generated in the Earth through time, less heat is also being convected to the surface. Thus, the vigor of mantle convection decreases with the age of the Earth. Since the strength of convection is dependent on viscosity, and the viscosity of the mantle is a sensitive function of its temperature, a decrease in the heat flux with time leads to a decrease in the mean mantle temperature. This cooling of the Earth in turn contributes to the surface heat flow. We consider this problem in detail in Chapter 13, and estimate that about 80% of the present surface heat flow can be attributed to the decay of radioactive isotopes presently in the Earth while about 20% comes from the cooling of the Earth. If we reduce the above upper bound to the present mantle heat production rate accordingly, we obtain $H = 7.38 \times 10^{-12}\,\text{W}\,\text{kg}^{-1}$ as an estimate of the actual present mean rate of radiogenic heat production per unit mass in the mantle.

Radioactive heating of the mantle and crust is attributed to the decay of the uranium isotopes ^{235}U and ^{238}U, the thorium isotope ^{232}Th, and the potassium isotope ^{40}K. The rates of heat production and the half-lives $\tau_{1/2}$ of these isotopes are given in Table 4.2. At the present time natural uranium is composed of 99.28% by weight ^{238}U and 0.71% ^{235}U. Natural thorium is 100% ^{232}Th. Natural potassium is composed of 0.0119% ^{40}K. The present rates of heat production of natural uranium and potassium are also given in Table 4.2.

The ratios of potassium to uranium and thorium to uranium are nearly constant in a wide range of terrestrial rocks. Based on these observed ratios we take $C_0^{\text{K}}/C_0^{\text{U}} = 10^4$ and $C_0^{\text{Th}}/C_0^{\text{U}} = 4$, where C_0^{K}, C_0^{Th}, and C_0^{U} are the present mass concentrations of potassium, thorium, and uranium, respectively. The total present heat production rate per unit mass H_0

Table 4.2. *Rates of Heat Release H and Half-lives $\tau_{1/2}$ of the Important Radioactive Isotopes in the Earth's Interior[a]*

Isotope	H $(\text{W}\,\text{kg}^{-1})$	$\tau_{1/2}$ (yr)	Concentration, C $(\text{kg}\,\text{kg}^{-1})$
^{238}U	9.46×10^{-5}	4.47×10^{9}	30.8×10^{-9}
^{235}U	5.69×10^{-4}	7.04×10^{8}	0.22×10^{-9}
U	9.81×10^{-5}		31.0×10^{-9}
^{232}Th	2.64×10^{-5}	1.40×10^{10}	124×10^{-9}
^{40}K	2.92×10^{-5}	1.25×10^{9}	36.9×10^{-9}
K	3.48×10^{-9}		31.0×10^{-5}

[a] Heat release is based on the present mean mantle concentrations of the heat-producing elements.

is related to the heat generation rates of the individual radioactive elements by

$$H_0 = C_0^U \left(H^U + \frac{C_0^{Th}}{C_0^U} H^{Th} + \frac{C_0^K}{C_0^U} H^K \right) \tag{4.1.40}$$

With $H_0 = 7.38 \times 10^{-12}$ W kg^{-1} and the other parameters as given above and in Table 4.2, we find that $C_0^U = 3.1 \times 10^{-8}$ kg kg^{-1} or 31 ppb (parts per billion by weight). These preferred values for the mean mantle concentrations of heat-producing elements are also given in Table 4.2.

The mean heat production rate of the mantle in the past can be related to the present heat production rate using the half-lives of the radioactive isotopes – see Section 12.4.1. The concentration C of a radioactive isotope at time t measured backward from the present is related to the present concentration C_0 and the half-life of the isotope $\tau_{1/2}$ by

$$C = C_0 \exp\left(\frac{t \ln 2}{\tau_{1/2}} \right) \tag{4.1.41}$$

Thus, the past mean mantle heat production rate is given by

$$\begin{aligned}
H = {} & 0.9927 C_0^U H^{238U} \exp\left(\frac{t \ln 2}{\tau_{1/2}^{238U}} \right) \\
& + 0.0072 C_0^U H^{235U} \exp\left(\frac{t \ln 2}{\tau_{1/2}^{235U}} \right) \\
& + C_0^{Th} H^{Th} \exp\left(\frac{t \ln 2}{\tau_{1/2}^{Th}} \right) \\
& + 1.28 \times 10^{-4} C_0^K H^{40K} \exp\left(\frac{t \ln 2}{\tau_{1/2}^{40K}} \right)
\end{aligned} \tag{4.1.42}$$

The rate of mean heat production based on (4.1.42) and parameter values in Table 4.2 is plotted as a function of time before the present in Figure 4.6. The past contributions of the individual radioactive elements are also shown. It can be seen that the rate of heat production 3 Gyr ago was about twice the present value. At the present time heat is produced primarily by ^{238}U and ^{232}Th, but in the distant past ^{235}U and ^{40}K were the dominant isotopes because of their shorter half-lives.

The concentrations of the heat-producing elements in surface rocks vary considerably. Some typical values are given in Table 4.3. The mantle values from Table 4.2 are included for reference. Partial melting at ocean ridges depletes mantle rock of incompatible elements such as uranium, thorium, and potassium. These incompatible elements are concentrated in the basaltic partial melt fraction. As a result, the oceanic crust (tholeiitic basalt) is enriched in these elements by about a factor of 4 relative to the undepleted mantle. Peridotites that have been depleted in the incompatible elements are sometimes found on the surface of the Earth. A typical example of the small concentrations of the heat-producing elements in a "depleted" peridotite is given in Table 4.3. Processes that lead to the formation of the continental crust, such as the volcanism associated with ocean trenches, further differentiate the incompatible elements. The concentrations of the heat-producing elements in a typical continental rock
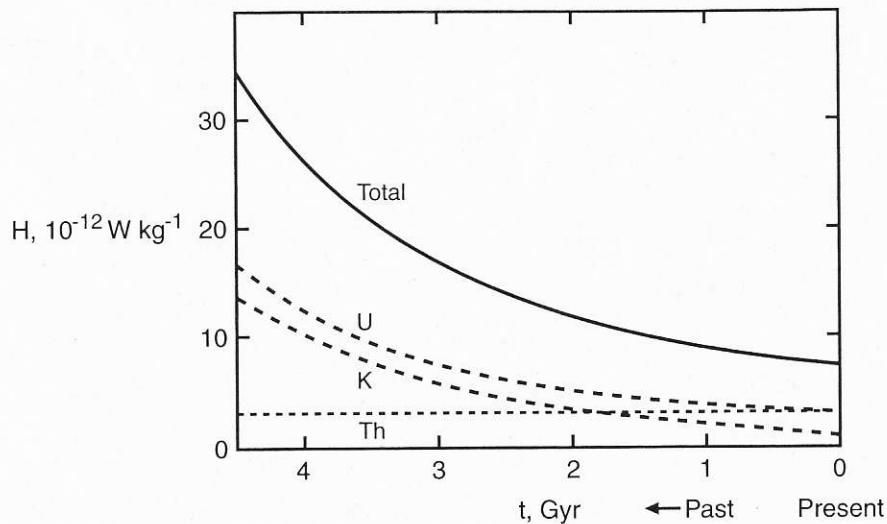
Figure 4.6. Mean mantle heat production rates due to the decay of the radioactive isotopes ^{238}U, ^{235}U, ^{232}Th, and ^{40}K as functions of time measured back from the present.

Table 4.3. *Typical Concentrations of the Heat-producing Elements in Several Rock Types and the Average Concentrations in Chondritic Meteorites*

Rock Type	Concentration		
	U (ppm)	Th (ppm)	K (%)
Reference undepleted mantle	0.031	0.124	0.031
"Depleted" peridotites	0.001	0.004	0.003
Tholeiitic basalt	0.9	2.7	0.83
Granite	4.7	20	4.2
Shale	3.7	12	2.7
Average continental crust	1.42	5.6	1.43
Chondritic meteorites	0.012	0.042	0.085

such as a granite are quite variable, but in general they are an order of magnitude greater than in tholeiitic basalts. Representative values of concentrations in granite are given in Table 4.3.

It is generally accepted that the chondritic class of meteorites is representative of primitive mantle material. The average concentrations of the heat-producing elements in chondritic meteorites are listed in Table 4.3. The concentrations of uranium and thorium are about a factor of 2 less than our mean mantle values, and the concentration of potassium is about a factor of 3 larger. The factor of 6 difference in the ratio C_0^K/C_0^U is believed to represent a fundamental difference in elemental abundances between the Earth's mantle and chondritic meteorites.

In the next two sections we will consider the structure of the upper thermal boundary layer comprising the oceanic and continental lithospheres. These boundary layers are relatively thin with thickness between 0 and about 200 km. In determining these thermal structures we will neglect adiabatic changes in temperature. Since the adiabatic gradient is only about 0.4 K km^{-1} this is a reasonable approximation. A systematic treatment of this approximation will be given in Chapter 6.

4.2 Thermal Regime of the Oceanic Lithosphere

The oceanic lithosphere is the upper thermal boundary layer of the convecting mantle. It is formed at accretional plate margins by the cooling of hot mantle rock. The oceanic lithosphere is convected away from ridge crests at the spreading rate deduced from the pattern of magnetic anomalies on the seafloor (see Chapter 2). The oceanic lithosphere thickens with time as the upper mantle cools by conduction and by hydrothermal heat loss to the oceans. The resulting thermal contraction produces an increase in seafloor depth with crustal age in the direction of seafloor spreading. Accompanying the increase in seafloor depth with crustal age are decreases in surface heat flow and a decreasing geoid height with age. It has been established that these trends do not continue unbroken onto the oldest oceanic lithosphere. Instead, there is a gradual transition in the vicinity of 70–100 Myr crustal ages, which appears to separate two different thermal boundary layer regimes. For crustal ages less than 70 Myr, the statistical variation in seafloor depth can be explained by a cooling half-space model. In this model, the depth of the water column, relative to its depth at the ridge crest, increases with the square root of the crustal age. The actual seafloor topography approximates this behavior at young ages (Parsons and Sclater, 1977). At greater ages, seafloor depth increases more slowly, on average. A similar trend is observed in geoid heights. The geoid height decreases linearly with crustal age to about 50 Myr in the North and South Atlantic and in the Indian Ocean (Sandwell and Schubert, 1980).

Interpretations of surface heat flow are more complex. Heat flow on the ocean floor is obtained from many thousands of point measurements and is subject to large variability. Variability in heat flow can be reduced by the careful selection of measurement sites and appropriate averaging (Sclater et al., 1980). For crustal ages between about 10 and 80 Myr the heat flow is inversely proportional to the square root of the crustal age, in agreement with the half-space cooling model.

Significant departures occur on young crust, presumably because of additional heat loss by hydrothermal circulation systems (Lister, 1980). There is also a significant departure from the predictions of the cooling half-space model for old ocean crust. Densely spaced heat flow measurements in the Pacific by Von Herzen et al. (1989) have suggested that the average heat flow on older ocean crust may also be higher than the heat flow predicted by the cooling half-space model, and this is substantiated in the data compiled by Stein and Stein (1992) (see also Stein and Stein, 1996).

4.2.1 Half-space Cooling Model

We first demonstrate that the temperature distribution in the oceanic lithosphere as determined using the cooling half-space model described in the previous section provides an adequate first-order model for ages less than about 80 Myr. The geometry is illustrated in Figure 4.7. Because of its low temperature, the lithosphere behaves as a rigid moving plate. The temperature in the plate is governed by the convection–conduction equation (see Chapter 6)

$$u_0 \frac{\partial T}{\partial x} = \kappa \left(\frac{\partial^2 T}{\partial x^2} + \frac{\partial^2 T}{\partial y^2} \right) \tag{4.2.1}$$

where u_0 is the velocity of seafloor spreading. The Peclét number for the oceanic lithosphere is defined by $Pe \equiv u_0 L / \kappa$, where L is a typical distance from the ocean ridge. With $u_0 = 50 \, \text{mm yr}^{-1}$, $L = 1{,}000 \, \text{km}$, and $\kappa = 1 \, \text{mm}^2 \, \text{s}^{-1}$ as typical values, we find $Pe = 1{,}600$.
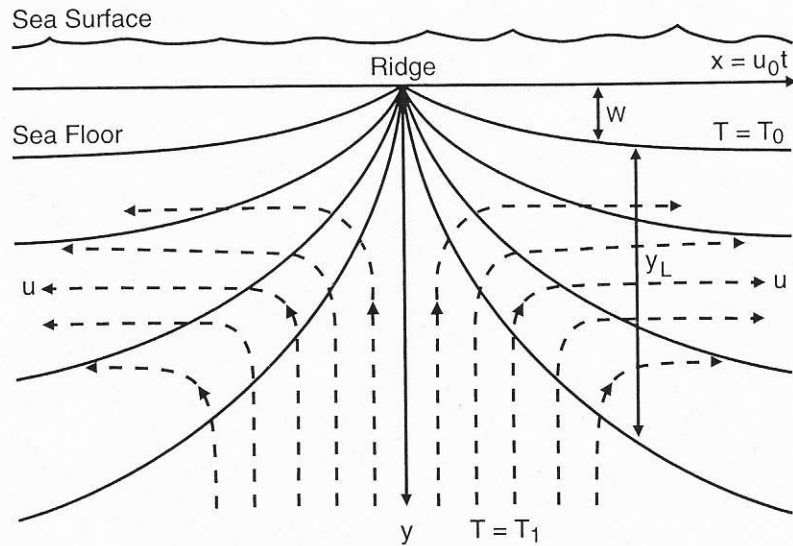
Figure 4.7. A sketch showing the model of oceanic lithosphere formation by seafloor spreading from a mid-ocean ridge used to derive the thermal boundary layer cooling curves. Solid contours are isotherms; dashed contours are streamlines. The depth to the subsiding seafloor w and the thickness of the lithosphere y_L are shown.

For a large Peclét number it is appropriate to make the boundary layer approximation and neglect horizontal heat conduction compared with vertical heat conduction, and (4.2.1) becomes

$$u_0 \frac{\partial T}{\partial x} = \kappa \frac{\partial^2 T}{\partial y^2} \tag{4.2.2}$$

Since $t = x/u_0$ we can rewrite (4.2.2) as

$$\frac{\partial T}{\partial t} = \kappa \frac{\partial^2 T}{\partial y^2} \tag{4.2.3}$$

which is identical to (4.1.1). The required initial and boundary conditions are $T = T_1$ at $t = 0$, $T = T_0$ at $y = 0$, and $T \to T_1$ as $y \to \infty$. Thus, the solution given in (4.1.20) is valid and the temperature distribution in the oceanic lithosphere is

$$\frac{T_1 - T}{T_1 - T_0} = \text{erfc}\left(\frac{y}{2(\kappa t)^{1/2}}\right) \tag{4.2.4}$$

Isotherms as a function of depth and age are given in Figure 4.8 for $T_1 - T_0 = 1{,}300\,\text{K}$ and $\kappa = 1\,\text{mm}^2\,\text{s}^{-1}$.

From (4.1.23), the surface heat flow q_0 as a function of age t is given by

$$q_0 = \frac{k(T_1 - T_0)}{(\pi \kappa t)^{1/2}} \tag{4.2.5}$$

For $k = 3.3\,\text{W m}^{-1}\,\text{K}^{-1}$ and other values as above, the surface heat flow is related to the age of the seafloor t by

$$q_0 = \frac{431}{\sqrt{t}} \tag{4.2.6}$$

Mantle Temperatures and Thermodynamic Properties
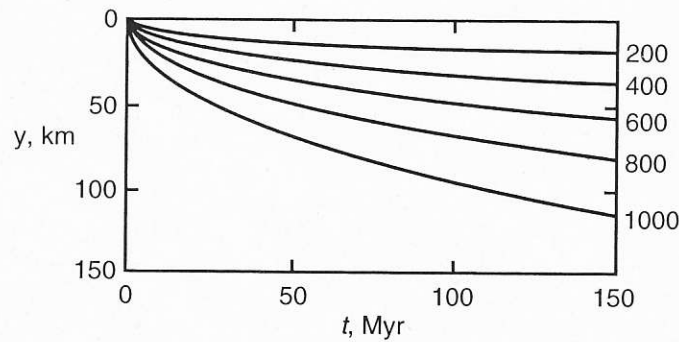
Figure 4.8. Isotherms as a function of depth and age in the oceanic lithosphere from (4.2.4) taking $T_1 - T_0 = 1,300\,\text{K}$ and $\kappa = 1\,\text{mm}^2\,\text{s}^{-1}$. The isotherms are values of $T - T_0$ in K.
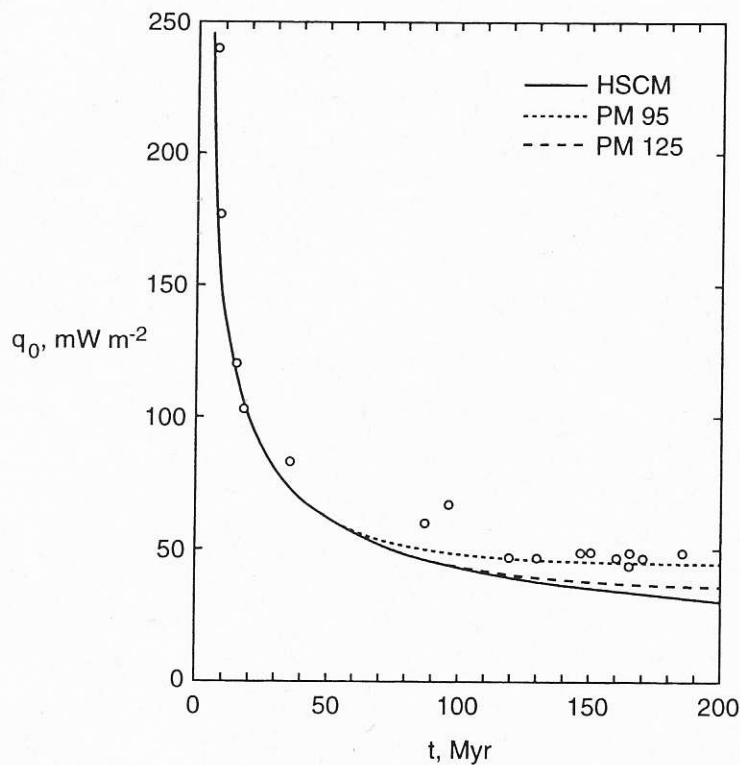
Figure 4.9. Heat flow as a function of the age of the ocean floor. The data points are from sediment-covered regions of the Atlantic and Pacific Oceans (Lister et al., 1990). Comparisons are made with the half-space cooling model (HSCM) from (4.2.6) and the plate model from (4.2.29) with $y_{L0} = 95\,\text{km}$ (PM95) and with $y_{L0} = 125\,\text{km}$ (PM125).

with t in Myr and q in $\text{mW}\,\text{m}^{-2}$. This result is compared with measurements of heat flow compiled by Lister et al. (1990) in Figure 4.9. Many measurements of the heat flow through the ocean floor have been carried out and, in general, they have a great deal of scatter (Stein and Stein, 1992, 1996). A major cause of this scatter is hydrothermal circulation through the oceanic crust. The heat loss associated with these circulations causes observed heat flows to be systematically low. Because of this problem, Lister et al. (1990) considered only measured values in thick sedimentary cover that would inhibit hydrothermal circulations. The heat flow predicted by the half-space cooling model is in reasonable agreement with the data, but it is somewhat less than the measured values.

The thickness of the oceanic lithosphere from (4.1.22) is

$$y_L = 2.32 \, (\kappa t)^{1/2} \qquad (4.2.7)$$

For our nominal value of $\kappa = 1 \, \text{mm}^2 \, \text{s}^{-1}$, the thickness of the lithosphere in km is related to the seafloor age in Myr by

$$y_L = 13\sqrt{t} \qquad (4.2.8)$$

With $t = 10 \, \text{Myr}$ we have $y_L = 41 \, \text{km}$ and with $t = 100 \, \text{Myr}$ we have $y_L = 130 \, \text{km}$. It should be emphasized that the thickness given in (4.2.7) is arbitrary in that it corresponds to $(T_1 - T)/(T_1 - T_0) = 0.9$.

The temperature distribution in the oceanic lithosphere can also be used to predict the morphology of oceanic ridges. As the oceanic lithosphere thickens, its temperature decreases and its density increases due to thermal contraction. The heavier lithosphere sags downward, thus deepening the oceans with increasing distance from the ridge. The depth of the ocean as a function of crustal age can be found by the application of the principle of isostasy, based on an assumed hydrostatic equilibrium. The principle of isostasy states that there is the same mass per unit area between the surface and some depth of compensation for any vertical column of material. This is equivalent to the assumption that the lithostatic pressure at some depth is horizontally homogeneous.

The mass per unit area in a column of any age is

$$\int_0^{y_L} \rho \, dy + w \rho_w$$

where y_L is the thickness of the lithosphere, ρ_w is the density of water, and w is the depth of the ocean floor below the ridge crest. At the ridge crest, $\rho = \rho_1$ the deep mantle density, and the mass of a column of vertical height $w + y_L$ is $\rho_1 (w + y_L)$. Hydrostatic equilibrium requires that

$$w \, (\rho_w - \rho_1) + \int_0^{y_L} (\rho - \rho_1) \, dy = 0 \qquad (4.2.9)$$

The first term in (4.2.9) represents a negative mass because water with density ρ_w is less dense than the mantle rock it has replaced because of the subsidence of the seafloor a distance w. The second term in the equation represents a positive mass because thermal contraction in the cooling lithosphere causes the density ρ to be higher than the reference hot mantle rock density ρ_1. Introduction of the volume coefficient of thermal expansion α allows us to write

$$\rho - \rho_1 = \rho_1 \alpha \, (T_1 - T) \qquad (4.2.10)$$

Upon substitution of the temperature profile from (4.2.4) into (4.2.10) and further substitution of the result into (4.2.9), we obtain

$$w \, (\rho_1 - \rho_w) = \rho_1 \alpha \, (T_1 - T_0) \int_0^\infty \text{erfc}\left[\frac{y}{2\sqrt{\kappa t}}\right] dy \qquad (4.2.11)$$

Since $\rho \to \rho_1$ and $T \to T_1$ at the base of the lithosphere, the limit on the integral has been changed from $y = y_L$ to $y = \infty$. We can rewrite (4.2.11) using (4.1.3) with the result

$$w = \frac{2\rho_1 \alpha \, (T_1 - T_0)}{(\rho_1 - \rho_w)} \, (\kappa t)^{1/2} \int_0^\infty \text{erfc}(\eta) \, d\eta \qquad (4.2.12)$$

The definite integral has the value

$$\int_0^\infty \mathrm{erfc}(\eta)\, d\eta = \frac{1}{\sqrt{\pi}} \qquad (4.2.13)$$

so that

$$w = \frac{2\rho_1 \alpha \, (T_1 - T_0)}{(\rho_1 - \rho_w)} \left(\frac{\kappa t}{\pi} \right)^{1/2} \qquad (4.2.14)$$

Equation (4.2.14) predicts that the depth of the ocean increases with the square root of the age of the ocean floor. For $\rho_1 = 3{,}300\,\mathrm{kg\,m^{-3}}$, $\rho_w = 1{,}000\,\mathrm{kg\,m^{-3}}$, $\kappa = 1\,\mathrm{mm^2\,s^{-1}}$, $T_1 - T_0 = 1{,}300\,\mathrm{K}$, and $\alpha = 3 \times 10^{-5}\,\mathrm{K^{-1}}$, the ocean subsidence w in km is related to the seafloor age in Myr by

$$w = 0.35\sqrt{t} \qquad (4.2.15)$$

With $t = 10\,\mathrm{Myr}$ we have $w = 1.1\,\mathrm{km}$ and with $t = 100\,\mathrm{Myr}$ we have $w = 3.5\,\mathrm{km}$. This result with a ridge depth of 2.5 km is compared with seafloor depths in the oceans in Figure 4.10. For this comparison we have chosen the depths given by Johnson and Carlson (1992) obtained from DSDP (Deep Sea Drilling Program) and ODP (Ocean Drilling Program) drill sites. Corrections have been made for sediment thickness, and "normal" crust in the Atlantic, Pacific, and Indian Oceans is considered. Other comprehensive compilations of ocean depth data have been given by Renkin and Sclater (1988) and by Kido and Seno (1994) with similar results.

For seafloor ages of less than about 80 Myr the data correlate well with the half-space cooling model result given in (4.2.15). At ages greater than about 80 Myr the seafloor is
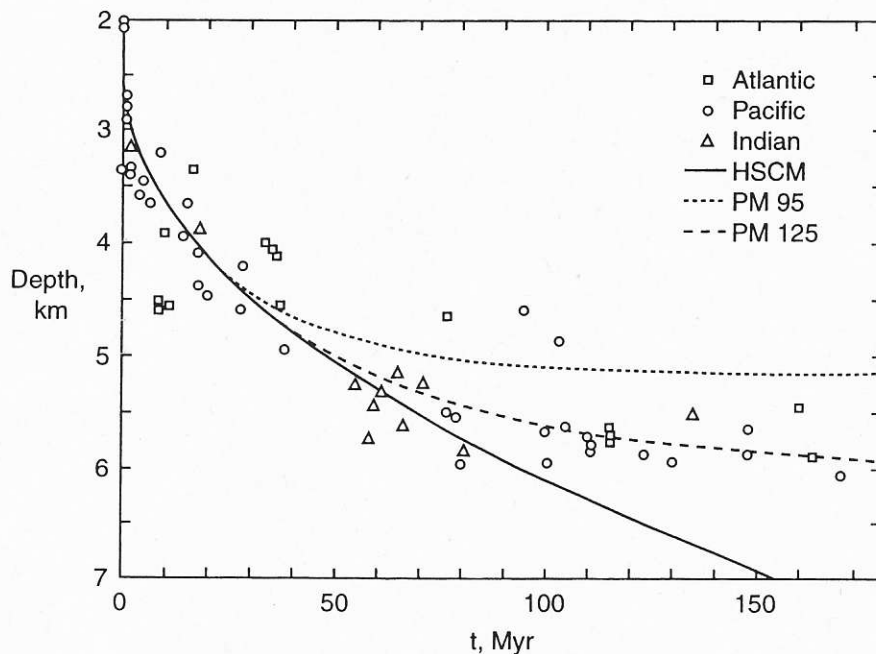
Figure 4.10. Seafloor depth as a function of age in the Atlantic, Pacific, and Indian Oceans. Data are from DSDP and ODP drill sites on normal ocean crust and depths have been corrected for sediment cover (Johnson and Carlson, 1992). Comparisons are made with the half-space cooling model (HSCM) from (4.2.15) and the plate model from (4.2.32) with $y_{L0} = 95\,\mathrm{km}$ (PM95) and with $y_{L0} = 125\,\mathrm{km}$ (PM125).

systematically shallower than the half-space cooling model prediction. The topography data in Figure 4.10 have much less scatter than the heat flow data in Figure 4.9, perhaps because the topography is an integral measure of the entire thermal structure of the lithosphere rather than the near-surface thermal gradient contaminated by hydrothermal effects.

We next consider a third independent measure of the thermal structure of the oceanic lithosphere. The Earth's gravitational field is a measure of the density distribution within the Earth. As discussed above in connection with seafloor subsidence, it is appropriate to assume isostatic equilibrium for the oceanic lithosphere. Haxby and Turcotte (1978) showed that the surface gravitational potential anomaly ΔU due to a shallow, long-wavelength isostatic density distribution is proportional to the dipole moment of the density distribution beneath the point of measurement:

$$\Delta U = 2\pi G \int_0^h y \Delta\rho(y)\, dy \qquad (4.2.16)$$

where G is the gravitational constant, h is the depth of compensation, and $\Delta\rho(y)$ is the difference between the density $\rho(y)$ and a reference density.

The gravitational potential anomaly can be related directly to the geoid anomaly ΔN by

$$\Delta U = -g\Delta N \qquad (4.2.17)$$

The geoid anomaly is the vertical distance between the actual equipotential surface of the Earth and the reference spheroid. Substitution of (4.2.17) into (4.2.16) gives

$$\Delta N = -\frac{2\pi G}{g} \int_0^h y \Delta\rho\,(y)\, dy \qquad (4.2.18)$$

With the mantle density beneath the oceanic ridge taken as the reference density ($\Delta\rho = \rho - \rho_1$), the geoid anomaly associated with the subsiding, thermally compensated oceanic lithosphere can be written as

$$\Delta N = \frac{-2\pi G}{g} \left\{ \int_{-w}^0 y\,(\rho_w - \rho_1)\, dy + \int_0^\infty y\,(\rho - \rho_1)\, dy \right\} \qquad (4.2.19)$$

The first term on the right side of (4.2.19) can be integrated directly and the second term can be rewritten using (4.2.10) relating density to temperature. The result is

$$\Delta N = \frac{-2\pi G}{g} \left\{ \frac{(\rho_1 - \rho_w)\, w^2}{2} + \alpha\rho_1 \int_0^\infty y\,(T_1 - T)\, dy \right\} \qquad (4.2.20)$$

By using (4.2.14) for the ocean floor depth w and (4.2.4) for the temperature distribution in the lithosphere, we can obtain the following simple formula for the geoid anomaly over a spreading ridge:

$$\Delta N = -\frac{2\pi G \rho_1 \alpha\kappa\,(T_1 - T_0)}{g} \left\{ 1 + \frac{2\rho_1\alpha\,(T_1 - T_0)}{\pi\,(\rho_1 - \rho_w)} \right\} t \qquad (4.2.21)$$

This geoid anomaly is a linear function of the age of the seafloor. For $\rho_1 = 3{,}300\,\mathrm{kg\,m^{-3}}$, $\kappa = 1\,\mathrm{mm^2\,s^{-1}}$, $T_1 - T_0 = 1{,}300\,\mathrm{K}$, and $\alpha = 3 \times 10^{-5}\,\mathrm{K^{-1}}$, we find that the geoid anomaly ΔN in m is related to the age t in Myr by

$$\Delta N = -0.18t \qquad (4.2.22)$$

With $t = 10\,\mathrm{Myr}$ the geoid anomaly is $\Delta N = -1.8\,\mathrm{m}$ and with $t = 100\,\mathrm{Myr}$ the geoid anomaly is $\Delta N = -18\,\mathrm{m}$.
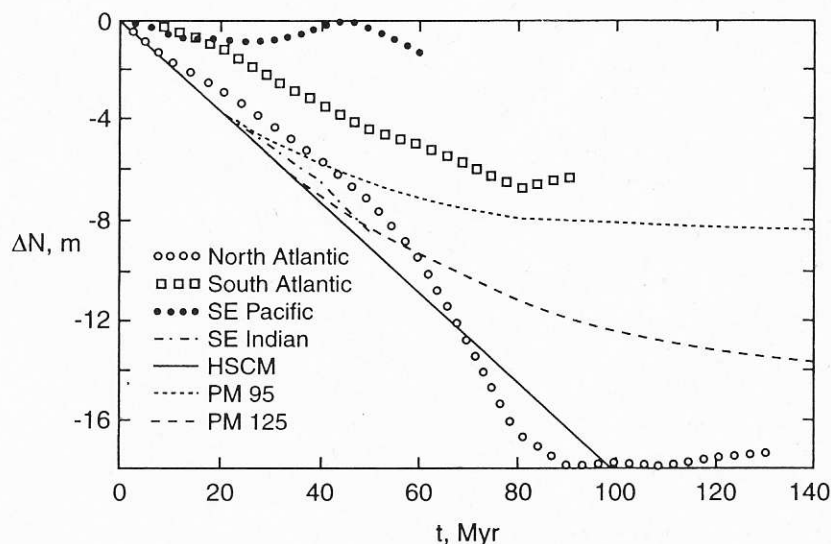
Figure 4.11. Geoid anomalies relative to ridge crests are given as a function of seafloor age for the North Atlantic, South Atlantic, SE Pacific, and SE Indian Oceans (Sandwell and Schubert, 1980). Comparisons are made with the half-space cooling model (HSCM) from (4.2.22) and the plate cooling model from (4.2.35) with $y_{L0} = 95\,\mathrm{km}$ (PM95) and with $y_{L0} = 125\,\mathrm{km}$ (PM125).

Over the oceans the sea surface represents an equipotential surface to a first approximation. Deviations are due to tides, ocean currents, and storms. Laser altimeter measurements of the sea surface from satellites define the geoid over the oceans and provide maps of geoid anomalies. Geoid anomalies as a function of seafloor age for several oceans are given in Figure 4.11 (Sandwell and Schubert, 1980). Also included in the figure is the linear prediction from (4.2.22). Reasonably good agreement is found between theory and the data for the Southeast Indian and North Atlantic Oceans, but there is considerably more scatter than with the topography data. This scatter can be attributed to the geoid anomalies caused by deeper density anomalies in the mantle. This problem has also been considered in detail by Richardson et al. (1995).

The oceanic lithosphere on the two sides of a fracture zone ideally has a constant age difference $t_2 - t_1$. Associated with this age difference is an offset in the geoid. If the half-space cooling model is valid, then the offset in the geoid $\Delta N_2 - \Delta N_1$ is related to the age difference across the fracture zone $t_2 - t_1$ by (4.2.22) with the result

$$\frac{\Delta N_2 - \Delta N_1}{t_2 - t_1} = -0.18\,\mathrm{m\,Myr^{-1}} \qquad (4.2.23)$$

The ratio of geoid offset to the age difference across a fracture zone is predicted to be a constant (Detrick, 1981; Sandwell and Schubert, 1982; Cazenave et al., 1983; Cazenave, 1984; Driscoll and Parsons, 1988; Marty et al., 1988; Freedman and Parsons, 1990). Ratios of geoid offset to age difference, $(\Delta N_2 - \Delta N_1)/(t_2 - t_1)$, for the Mendocino fracture zone are given in Figure 4.12 as a function of the mean age of the crust at the fracture zone, $\bar{t} = (t_1 + t_2)/2$. The data are from Sandwell and Schubert (1982) and from Marty et al. (1988). Although there is considerable scatter, the magnitude of the geoid offset–age difference ratio appears to systematically decrease from the value predicted by (4.2.23) at older ages.

Observations of surface heat flow, bathymetry, and geoid are all in quite good agreement with the half-space cooling model for ages less than about 80 Myr. The bathymetry data
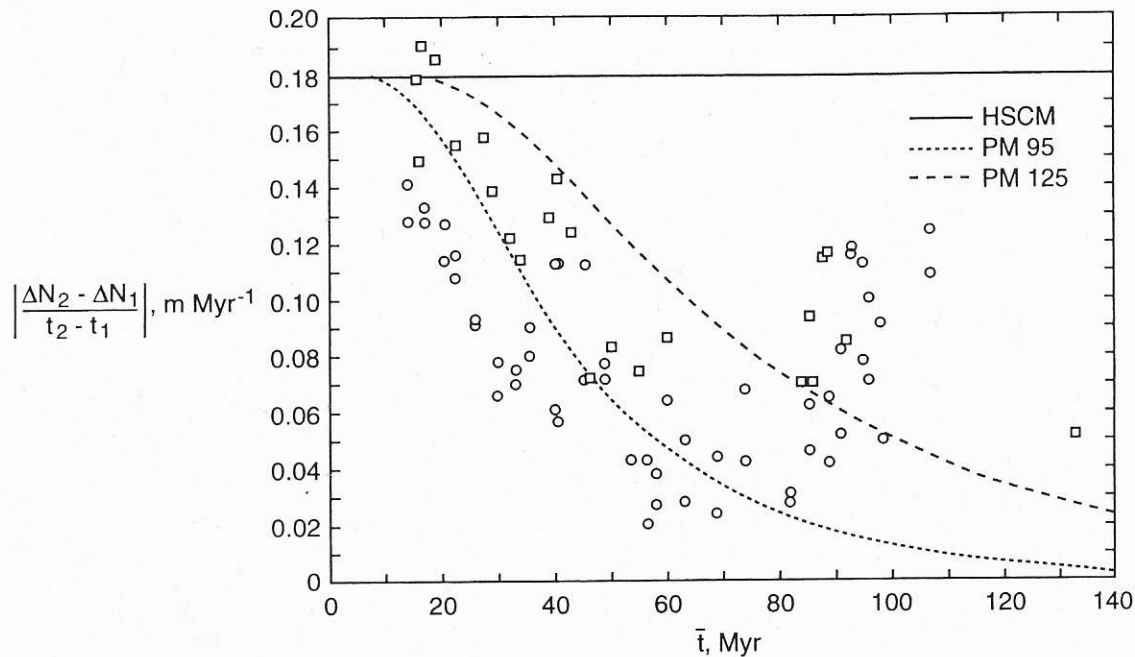
Figure 4.12. Magnitude of the ratio of the geoid offset $\Delta N_2 - \Delta N_1$ to the age difference $t_2 - t_1$ across the Mendocino fracture zone as a function of the mean age of the seafloor $\bar{t} = (t_1 + t_2)/2$. The squares are the data of Sandwell and Schubert (1982) and the circles are the data of Marty et al. (1988). Comparisons are made with the half-space cooling model (HSCM) from (4.2.23) and with the plate cooling model from (4.2.36) with $y_{L0} = 95$ km (PM95) and with $y_{L0} = 125$ km (PM125).

show the least scatter and show a clear flattening of the bathymetry versus age curves at greater ages.

Question 4.1: Why are there deviations from the half-space cooling model for the oceanic lithosphere at seafloor ages greater than about 80 Myr?

4.2.2 *Plate Cooling Model*

As discussed above, observational evidence indicates that the oceanic lithosphere does not continue to thicken with age at ages greater than 60–100 Myr as predicted by the half-space cooling model. The physical explanation is that basal heating of the oceanic lithosphere occurs either due to the impingement of plumes or due to secondary convection. A model for this process is provided by the cooling of a finite thickness plate (McKenzie, 1967).

The constant thickness of the plate is prescribed to be y_{L0}, the thickness of the lithosphere at large times. At the surface of the plate the temperature is the water temperature T_0 ($T = T_0$ at $y = 0$); at the base of the plate the temperature is the mantle temperature T_1 ($T = T_1$ at $y = y_{L0}$). Initially at the ridge, $x = t = 0$, the temperature is the mantle temperature ($T = T_1$ at $t = 0$). We require the solution of the heat conduction equation (4.2.3) that satisfies these boundary conditions. Carslaw and Jaeger (1984, p. 100) have given the appropriate solution in the form of an infinite series

$$T = T_0 + (T_1 - T_0) \left[\frac{y}{y_{L0}} + \frac{2}{\pi} \sum_{n=1}^{\infty} \frac{1}{n} \exp\left(-\frac{\kappa n^2 \pi^2 t}{y_{L0}^2} \right) \sin\left(\frac{n\pi y}{y_{L0}} \right) \right] \qquad (4.2.24)$$